

Plasmon Modes of Nanosphere Trimers and Quadrumers

Daniel W. Brandl,[†] Nikolay A. Mirin,[‡] and Peter Nordlander^{*,†}

Department of Physics and Astronomy M.S. 61, and Chemistry M.S. 60, and the Laboratory for Nanophotonics, LANP, Rice University, Houston, Texas 77251-1892

Received: March 3, 2006; In Final Form: April 18, 2006

Using the plasmon hybridization method, we investigate the plasmon frequencies and optical absorption spectra of symmetric configurations of nanosphere trimers and quadrumers. Plasmon hybridization allows us to express the fundamental plasmon modes of these multinanoparticle systems as linear combinations of the plasmons of individual nanospheres in a manner analogous to molecular orbital theory. We show how group theory may be used to interpret the plasmon modes of each multiparticle system as specific structure-dependent symmetric combinations of the plasmon modes of the individual nanoparticles. We compare the optical absorption spectra calculated using plasmon hybridization with the spectra obtained using finite difference time domain simulations.

I. Introduction

The discovery of surface-enhanced Raman spectroscopy (SERS) has led to a number of studies of the plasmonic properties of nanoparticles.^{1–7} This interest is due in part to large local electric field enhancements that are induced near nanoparticle surfaces upon excitation of their plasmons. SERS cross sections can depend of the fourth power of the electric field across a target molecule when the wavelengths of the incident and scattered photons are near the plasmon resonance of a substrate. Thus, high field enhancements near nanoparticles can potentially provide for greatly increased SERS efficiency, as has been demonstrated recently for dimers.^{8–10}

The electric-field enhancements induced by surface plasmons depend greatly on the shape of the nanoparticle.¹¹ Field enhancements of single dipolar particles are typically of an order of magnitude, whereas those in the junctions of nanoparticle aggregates can be as large as 3 orders of magnitude.¹² In the systems that will be investigated in the present study, the maximum electric field enhancements are at least 2 orders of magnitude for both the symmetric trimer and symmetric quadruimer. In contrast, an individual nanosphere has a maximum electric field enhancement of only around 20. The collective effects associated with the interactions of plasmons in different nanoparticles thus lead to very strong enhancements. Because of these large field enhancements, nanoparticle aggregates are of particular importance as substrates in SERS.

Despite the existence of large electric field enhancements and their relevance to SERS, there have been few theoretical studies on the nature of the plasmon modes in multi-particle systems.^{13–18} In a recent paper, we extended the plasmon hybridization method to treat the plasmonic properties of nanoparticle dimers including the effects of dielectric backgrounds.¹⁹ In that application, we focused on symmetric nanosphere and nanoshell dimers and found excellent agreement with results from other theoretical methods.

The present paper extends the formalism developed previously for nanoshell dimers¹⁹ to arbitrary structures composed of a finite number of nanoparticles. We apply this formalism to study the plasmons of an equilateral nanoparticle trimer and an equilateral nanoparticle quadruimer. The results show that as the nanoparticle separation decreases, the plasmons of individual nanoparticles begin to interact and hybridize with the plasmons of the other particles. These interactions are not diagonal in the multipolar order of the individual nanoparticle plasmons, and for small interparticle separation, all plasmon modes of the combined system contain finite amounts of all multipolar order plasmons of the individual nanoparticles. This hybridization introduces a finite dipolar component into many of the plasmon modes of the combined system, making them dipole active and visible by light in the small-particle limit. This hybridization behavior is reminiscent of the situation for nanoparticle dimers, but the complexity of the hybridization is much more involved in the multinanoparticle case. We show how group theory can be used to classify the symmetry of each plasmon mode of the interacting system and help identify the modes with large dipole moments and large electromagnetic field enhancements. The role of symmetry in the present plasmonic problem is entirely analogous to its role in molecular orbital theory and represents a significant simplification in the analysis and understanding of extinction spectra.

In section II, we extend the plasmon hybridization formalism to take into account more than two nanoparticles that do not necessarily lie on the same axis. In section III, we will discuss the use of group theory to predict the linear combinations of individual nanoparticle plasmons that compose a plasmon of a symmetric nanoparticle aggregate. In section IV, we will show the results of plasmon hybridization for a symmetric nanosphere trimer and quadruimer configurations. In this section, we will use group theory to classify the plasmon modes using the irreducible representations of point groups. Finally, section V contains a comparison of optical absorption spectra calculated by the plasmon hybridization and finite difference time domain (FDTD) methods, electric field enhancements of each system calculated using FDTD, and a discussion of the effect of symmetry breaking on the plasmon resonances.

* To whom correspondence should be addressed. Phone: (713)348-5171. Fax: (713)348-4150. E-mail: nordland@rice.edu.

[†] Department of Physics and Astronomy.

[‡] Department of Chemistry.

II. Plasmon Hybridization for Multiple Off-Axis Spherical Particles

The plasmon hybridization method, which neglects retardation effects, is a method used to express the plasmon frequencies of a complex nanostructure in terms of simpler, primitive plasmon modes.^{18,20} These modes couple through electromagnetic interactions, and the resulting plasmons are expressed as linear combinations of the primitive plasmons. In previous papers, this method was used to study the plasmons of single and concentric nanoshells, nanoparticles on metallic surfaces and thin films, and nanosphere and nanoshell dimers.^{18–23}

The plasmon hybridization formalism introduced for the description of nanoshell dimers in the presence of dielectric backgrounds¹⁹ can be generalized directly to a system with more than two particles. The following descriptions refer directly to the formalism introduced in our nanoshell dimer paper.¹⁹ The sums over particles should be extended to include all particles present in the structure. For structures where the particles are not aligned with a single axis, couplings between primitive plasmons of differing azimuthal m values must be included in the formalism. Specifically, the interaction integral I should be evaluated as

$$I_{l,m,l',m'}^{ij}(R) = \frac{1}{R^2} \int \frac{Y_{l,m}(\Omega_i) Y_{l',m'}(\Omega_j)}{r_j^{l'+1}} dS_i \quad (1)$$

where the integration is centered on nanoshell i and done over a spherical surface of radius R . The quantity r_j is the distance from the center of a separate nanoshell j to a point on this surface. The potential energy term A should be taken,

$$A_{p,q} = \frac{4\pi R_p^2 R_q^2}{2l' + 1} \times \begin{bmatrix} \nu_l(R_p, R_q) & \text{for shell of } p \text{ equal to shell of } q \text{ and } (l, m) = (l', m') \\ I_{l,m,l',m'}^{ij}(R_p) R_q^{l'} & \text{for shell of } p \text{ not equal to shell of } q \\ 0 & \text{otherwise} \end{bmatrix} \quad (2)$$

In the presence of background dielectrics such as a dielectric embedding medium (ϵ_E) or a dielectric background polarizability of the metal in nanoparticle i ($\epsilon_{S,i}$), the surface charges should be calculated from

$$\sigma_{S,L,M,i} = \frac{1}{2L+1} [(\epsilon_E - \epsilon_{S,i})(L+1)x_i^{L+2}\tau_{C,L,M,i} + (\epsilon_E(L+1) + \epsilon_{S,i}L)\tau_{S,L,M,i}] - \sum_{l,m,j \neq i} \frac{1}{2l+1} [(\epsilon_E - \epsilon_{S,i})a_j^{l+2}\Delta_{L,M,l,m}^{ij}(b_i)\tau_{C,l,m,j} + (\epsilon_E - \epsilon_{S,i})b_j^{l+2}\Delta_{L,M,l,m}^{ij}(b_i)\tau_{S,l,m,j}] \quad (3)$$

and similarly for the cavity term. The quantity $\Delta(R)$ is defined as before, i.e., as the derivative of the interaction integral,

$$\Delta_{l,m,l',m'}^{ij}(R) = \frac{\partial}{\partial R} I_{l,m,l',m'}^{ij}(R) = \frac{l}{R} I_{l,m,l',m'}^{ij}(R) \quad (4)$$

but with an additional azimuthal m' . The indices p and q now additionally run through all m indices. In the present paper, we are concerned with structures composed of solid nanospheres. The nanosphere limit is obtained from the nanoshell formalism by taking the limit of the inner radius of the shell to be zero

and discarding the amplitudes C_{lm} for the primitive cavity plasmon modes.

The plasmon modes of the symmetric nanosphere trimer and quadramer are obtained as linear expansions of individual nanosphere plasmon modes (primitive plasmons) by a diagonalization of the Lagrangian for the interacting system. The individual nanosphere plasmons modes have degeneracies of $2l+1$ and frequencies

$$\omega_{S,lm} = \omega_B \sqrt{l/(\epsilon_S + (l+1)\epsilon_E)} \quad (5)$$

For practical reasons, the expansion of the nanoparticle aggregate plasmons in terms of primitive plasmon modes must be terminated at a finite l_{\max} . The l_{\max} required for convergence depends on the interparticle separation. For the structures and interparticle separations studied in the present paper, it is sufficient to include all individual nanosphere plasmon modes up to multipolar order $l_{\max} = 20$.

III. Group Theory and Plasmon Modes

The nanoparticle aggregates in which we are interested, the equilateral triangle and square, have structural symmetries that are described in terms of specific point groups, D_{3h} and D_{4h} , respectively. Due to the interparticle interactions, the plasmons are spatially distributed over the entire structure. However, the overall structure of the collective modes must be consistent with the symmetry of the system. The individual particle plasmon modes, which are expressed as spherical harmonic multipoles, do not provide a suitable basis with regards to the symmetry of the configuration. To resolve this difficulty, we introduce linear combinations of the individual plasmons in exactly the same way as in the case of linear combinations of atomic orbitals (LCAO).²⁴ In the latter situation, individual atomic orbitals are used in linear combinations to provide a symmetry-adapted basis set for molecular orbitals.

For a function to be consistent with a symmetry means to be an eigenfunction of every symmetry operator in its point group. The energy (ω^2) operator must commute with each symmetry operator because the system is invariant with respect to point group operations. Operators that commute, such as energy and symmetry operators, share a common set of eigenfunctions. For every symmetry operator, each eigenfunction belongs to one of the irreducible representations of a group; the representation determines the set of eigenvalues for classes of point group operations. If operators commute, the nondegenerate eigenfunctions for both operators must be exactly the same, which corresponds to the case of one-dimensional irreducible representations that do not appear more than once in the reducible representation. The case of degenerate energies corresponds to a multidimensional representation, and the physical states need to be taken as linear combinations of symmetry-adapted functions from that representation.

A general procedure exists for generating a symmetry-adapted basis set.^{24,25} These combinations can be constructed by applying the projection operators of a symmetry group to the original basis functions. Symmetry-adapted basis sets have two important properties. Their nondegenerate elements correspond to specific energy states of a system, and any overlap integral of the functions from different representations must vanish unless the direct product of representations contains a component symmetric with respect to all group operations.

Now we consider symmetry-adapted plasmons of an equilateral triangle and a square with particles in the corners, corresponding to symmetry groups D_{3h} and D_{4h} , respectively.

The simplest case of plasmonic interaction is the dipole oscillation, which is very important due to the strong dipole coupling to incoming electromagnetic waves. The reducible dipole representations of those systems readily split into the sets of irreducible representations given by $\Gamma_{\text{tri}} = A'_1 + A'_2 + 2E' + A''_2 + E''$ for the system with D_{3h} symmetry, and $\Gamma_{\text{quad}} = A_{1g} + A_{2g} + B_{1g} + B_{2g} + 2E_u + A_{2u} + B_{1u} + E_g$ for the system with D_{4h} symmetry. Each reduction formula contains the same number of variables in the irreducible representations as in the corresponding original representation. Each one-dimensional representation (A or B) defines a specific physical state of a system. The two-dimensional representations (E) define the basis set for pairs of degenerate states. For both the trimer and the quadrumer, the representations contain the same 2-fold degenerate representation twice, $2E'$ and $2E_u$, respectively. The direct products of these irreducible representations to themselves contain totally symmetric parts, A'_1 and A_{1g} , respectively. This means that each E defines a separate degenerate state, and each state is physically represented by a linear combination of *all* functions associated with the E state.

IV. Results

In the following two subsections, we present the plasmonic structure of a symmetric nanosphere trimer and quadrumer. The nanoparticles used here each have a radius of 10 nm, bulk plasmon frequency of $\omega_B = 9.5$ eV, and background metal dielectric coefficient $\epsilon_S = 5$, values corresponding to silver particles.

To illustrate the nature of the plasmon hybridization occurring in our structures, we find it useful to present results for interparticle separations ranging continuously from very small to relatively large separations. In the systems considered here with very small metallic spheres, retardation effects will only influence the interaction between the plasmons of one nanoparticle with the plasmons on the other nanoparticles, i.e., the splitting of the plasmon resonances resulting from bonding and antibonding combinations of individual nanoparticle plasmon modes. For the largest interparticle separations studied, 40 nm, the spatial extent of the system is less than a quarter of the wavelength of the optically active plasmon resonances and the splitting between bonding and antibonding modes around 0.1 eV. For a system of spatial extent of a quarter wavelength, retardation effects can reduce the interaction by around 10%. Thus, for our largest structures, the neglect of retardation effects only amount to an error of 0.01 eV.

A. Symmetric Equilateral Trimer. The system discussed here is composed of three identical nanospheres that lie at the vertexes of an equilateral triangle. The characteristic separation, D , for this configuration is defined as the center-to-center separation of any two nanospheres. Figure 1a shows the plasmon energy levels predicted by plasmon hybridization as a function of D . For large separation, where the interaction between the particles is small, the plasmon energies of the system are the $3(2l + 1)$ -fold degenerate plasmon energies of an individual nanosphere. For a finite separation, an interaction exists between all primitive nanosphere plasmons resulting in hybridized trimer plasmons containing admixtures of individual nanosphere plasmons of all l -multipolar orders. When we refer to the multipolar order of a trimer plasmon, we mean the multipolar order this particular plasmon would have in the limit of infinite separation.

As the nanoparticle separation decreases, bonding and antibonding combinations of the individual nanoparticle plasmons are formed. The lowest six curves derive from the dipolar $l = 1$ nanoparticle plasmons. Three of these plasmons are doubly

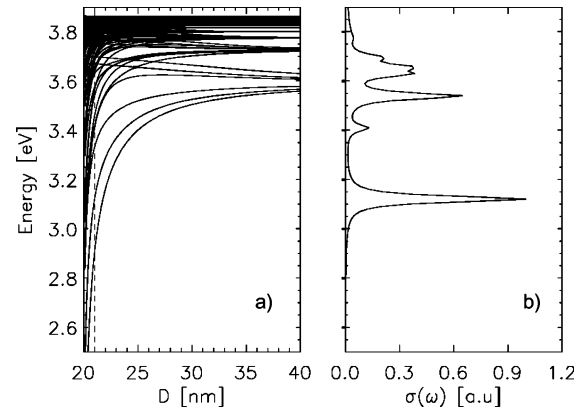


Figure 1. (a) All plasmon energies vs characteristic separation D of a trimer made up of silver nanospheres calculated using the plasmon hybridization method. (b) Optical absorption spectrum of the trimer at $D = 21$ nm (denoted by a dashed line on the left panel) for in-plane excitations as derived by plasmon hybridization. The nature of the in-plane plasmon modes is such that there is no azimuthal dependence (see Section V.A.). The broadening is taken to be small ($\delta = 0.015$ eV) so that the individual plasmon resonances can be distinguished.

degenerate. The next 10 curves derive from the quadrupolar $l = 2$ nanoparticle plasmons. The splitting of the bonding and antibonding plasmons of each l manifold becomes smaller with increasing l due to the decrease in the magnitude of the interactions. There are no avoided crossings of plasmons of different symmetries in this system, although plasmons of the same symmetry may exhibit these.

Figure 1b shows the optical absorption for this system at $D = 21$ nm for an in-plane excitation. The broadening is taken to be very small so that the individual trimer plasmon resonances may be observed. The figure shows that at this close nanoparticle separation, several different trimer plasmon modes are excited. The two lowest-energy peaks refer to $l = 1$ trimer plasmons. The higher-energy resonances are $l = 2$ and $l = 3$ trimer plasmons, which can be excited by light because of their admixture with the dipolar plasmon components from the individual nanospheres. The figure shows that several of the trimer plasmon resonances are absent from the absorption spectrum. For instance, the most redshifted $l = 1$ trimer plasmon resonance around 2.9 eV is not excited.

We observe that the trimer plasmon energy vs separation graph, which is obtained using a straightforward application of the plasmon hybridization formalism, is quite complicated and somewhat unenlightening when attempting to identify the physical origin of the bright modes shown in Figure 1b. There are two significant advantages that a group theory analysis of this system will provide. First, we may obtain symmetry-adapted linear combinations for the plasmon modes, the equivalent of LCAOs from molecular orbital theory, corresponding to each irreducible representation. This classification will aid in determining which trimer plasmon modes will be excitable by light and which will remain dark. Second, we may perform a basis change from our original matrix to one that is ordered by irreducible representation and l -multipolar order. Such a transformation renders the interaction matrix block diagonal with a significant reduction in numerical effort for its diagonalization.

The group theoretical approach allows us to separate the calculated trimer plasmon energy vs separation graph by irreducible representation. It is important to note that, despite the fact that there are interactions between different multipoles, there is no mixing of irreducible representations. Each plasmon mode has a single representation but a mixed l -multipolar composition. Put another way, plasmons mix into each other

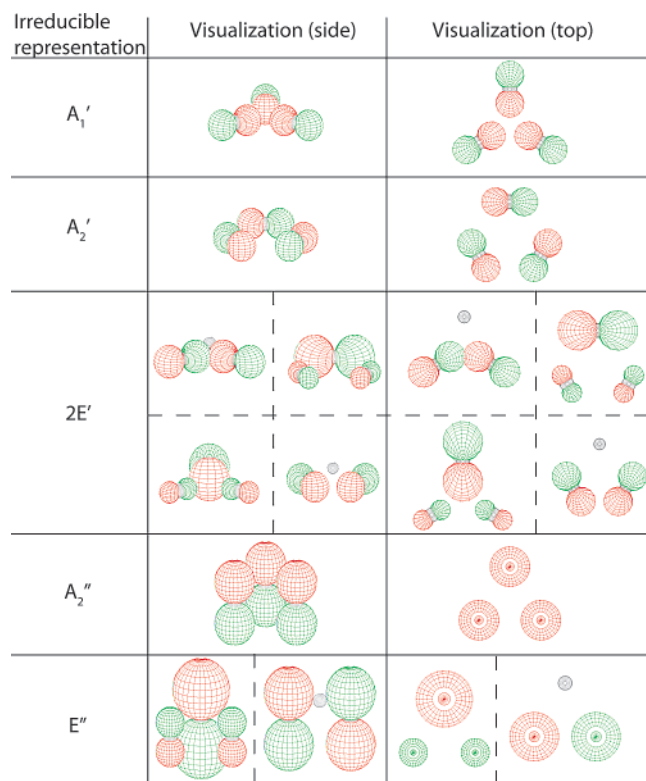


Figure 2. Irreducible representations and symmetric linear combinations of the $l = 1$ dipolar oscillations as predicted by group theory and plasmon hybridization.

with the same symmetries that they exhibit at infinite separation, i.e., where there is no multipolar mixing.

In the discussion of the trimer plasmons, we will focus on the symmetric linear combinations of nanoparticle dipolar plasmons because light couples most strongly to dipoles in the small-particle limit. As mentioned earlier, the reducible dipole representation splits into the sets of irreducible representations given by $\Gamma_{\text{tri}} = A_1' + A_2' + 2E' + A_2'' + E''$. We then use projection operators of the various irreducible representations present for dipoles to obtain the symmetric linear combinations associated with each representation. The projection operator for representation i is given by

$$\Pi_i = \frac{l_i}{h} \sum_R \chi_i(R) \times P_R \quad (6)$$

where l_i is the dimension of the representation, h is the dimension of the group, $\chi_i(R)$ is the character of the R th symmetry operator in the i representation, and P_R is the R th symmetry operator. The sum runs over all operators in the group. Applying this to the trimer gives us the linear combinations that are shown in Figure 2.

There are several things to note from the results of this analysis. The representations readily separate the trimer plasmon modes into in-plane (primed) and out-of-plane (double primed) modes. As previously noted, the one-dimensional representations correspond to the physical trimer plasmon modes. The one-dimensional in-plane modes can be described well in terms of oscillations radial to the center of the trimer and similar tangential oscillations. The representations A_1' and A_2' can then be understood as in-phase combinations of the radial or tangential components of the plasmons from each sphere, respectively. The lone one-dimensional out-of-plane representation, A_2'' , can be understood as an in-phase oscillation of all

dipoles out of the trimer plane. This implies that modes corresponding to A_1' and A_2' will be dark, because these have no in-plane dipole moment, and A_2'' modes will be bright for an out-of-plane excitation. The symmetric linear combinations of the dipoles for the two-dimensional E modes do not necessarily correspond to physical plasmons. However, these represent bases that may be used to describe the real physical trimer plasmons. For example, the in-plane mode that is excited at infinite separation, namely that with the dipole moments of all spheres aligned, can be represented as the sum of E' modes on the same row of Figure 2 in a linear combination which depends on the azimuthal excitation angle. The sum of the panels in the top row provides a state with all dipoles pointing to the side, and the sum of the bottom panels provides one with all dipoles pointing up.

It should be stressed that the physical in-plane modes are linear combinations of any of the four symmetries associated with E' , but each E' in the dipole representation refers to a separate doubly degenerate energy. Because the bases of E' modes have a dipole moment but the A' modes do not, any bright modes excited by in-plane excitations must correspond to E' symmetries. Similarly, the net out-of-plane dipole moment of the E'' basis is zero, and out-of-plane polarized light will only excite A_2'' modes.

Because there is no mixing of irreducible representation into the higher order modes, we may classify the trimer plasmons in Figure 1a according to their symmetry. Figure 3 shows the plasmon energy vs characteristic separation of the trimer plasmons up to multipolar order $l = 3$ for each irreducible representation. The figure shows that modes of the same representation have the same behavior when the characteristic separation is decreased. The plasmon resonances visible in Figure 1b correspond to excitations of the E' modes.

B. Symmetric Square Quadramer. The second system we study is composed of four identical nanospheres arranged in a square configuration. The characteristic separation we use to describe this system is the center-to-center separation of any two spheres on a side of the square. Figure 4 shows the quadramer plasmon energies found from the plasmon hybridization theory as a function of separation D for silver nanospheres and the calculated dipolar optical absorption for an in-plane excitation at $D = 21$ nm. As was the case for the trimer, bonding and antibonding combinations of the individual nanosphere plasmons are formed, resulting in a multitude of quadramer plasmon modes. For large separation D , the quadramer plasmons are the $4(2l + 1)$ -fold degenerate plasmon modes of the individual nanospheres. As the separation D decreases, the individual plasmons of each nanoparticle start to interact, resulting in quadramer plasmons containing finite admixtures of all primitive plasmon modes of the system. Although each quadramer plasmon contains a finite admixture of primitive plasmons of all multipolar indices l , they can be labeled with the multipolar l to which they merge in the limit of infinite separation D . The optical spectrum shown in Figure 4b indicates that several quadramer plasmon resonances can be excited by light. The most red-shifted $l = 1$ plasmon mode around 2.8 eV is not dipole active.

As was the case with the trimer, group theory provides a convenient means of understanding the nature of the plasmon modes of a quadramer. We will again restrict our discussion of symmetry-adapted functions to the dipolar plasmon modes. The dipolar component of a system with D_{4h} symmetry has a representation that splits into $\Gamma_{\text{quad}} = A_{1g} + A_{2g} + B_{1g} + B_{2g} + 2E_u + A_{2u} + B_{1u} + E_g$. Application of the symmetry operators

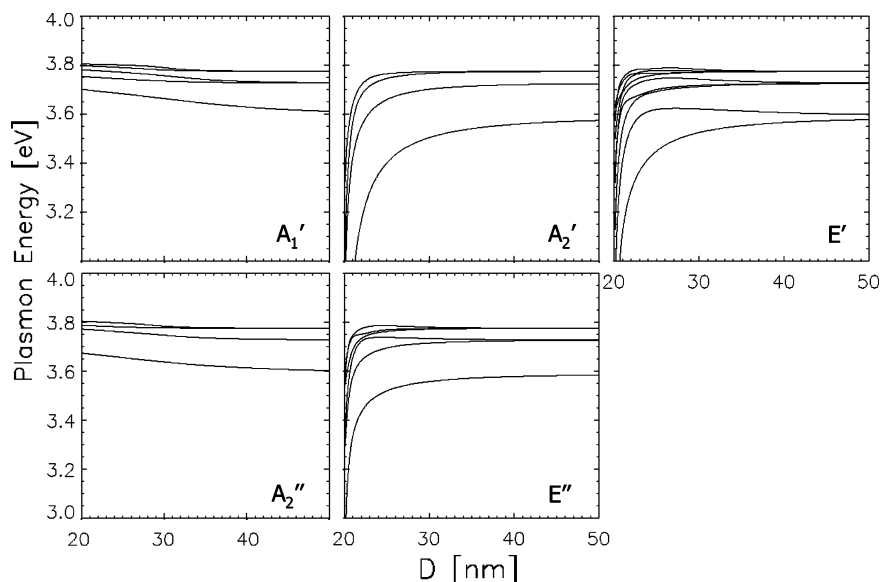


Figure 3. Plasmon energy vs characteristic separation for the nanosphere trimer described in Figure 1 up to $l = 3$ and classified by irreducible representation. Plasmon modes of E' symmetry can be excited by light polarized along the trimer plane and plasmon modes of A_2'' symmetry can be excited by light polarized perpendicular to the trimer plane.

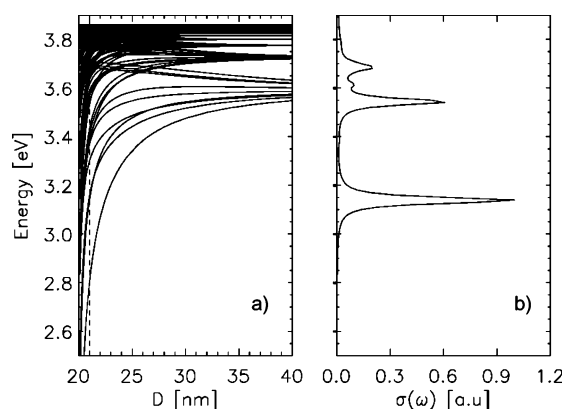


Figure 4. Plasmon energies vs characteristic separation for a quadramer made up of silver nanospheres ($r = 10$) calculated by plasmon hybridization (left), and the optical absorption spectrum for in-plane excitations at separation length $D = 21$ nm calculated by plasmon hybridization (right). The nature of the in-plane plasmon modes is such that there is no azimuthal dependence (see section V.A.). The broadening in the absorption spectra is taken to be small ($\delta = 0.015$ eV) so that the individual quadramer plasmon resonances may be distinguished.

results in the symmetric linear combinations shown in Figure 5. As with the trimer, the dipole representation readily splits into in-plane and out-of-plane symmetries. Again, the in-plane symmetries can be described as linear combinations of modes that are radial or tangential to the center of symmetry of the structure.

The four one-dimensional in-plane representations can be split into two sets of two representations each. The A_{1g} and A_{2g} representations can be described as in-phase oscillations of dipoles that are radial (A_{1g}) or tangential (A_{2g}) to the center. Representations B_{1g} and B_{2g} can be described as radial (B_{2g}) or tangential (B_{1g}) oscillations whose phases alternate with those of the next closest particle. None of these modes have a net dipole moment in any direction; therefore, the plasmon modes of these symmetries can be classified as dark. The in-plane modes that can be excited by light have symmetries from the E_u representation. A physical oscillation for such a mode can be expressed as a linear combination of the four modes belonging to that representation in Figure 5.

Irreducible representation	Visualization (side)	Visualization (top)
A_{1g}		
A_{2g}		
B_{1g}		
B_{2g}		
$2E_u$		
A_{2u}		
B_{1u}		
E_g		

Figure 5. Irreducible representations and symmetric linear combinations of the $l = 1$ dipolar oscillations of the quadramer predicted by group theory and plasmon hybridization.

The symmetries of the one-dimensional out-of-plane representations are similar to those of the one-dimensional in-plane representations. Symmetries corresponding to A_{2u} are in-phase, out-of-plane oscillations. The modes of the B_{1u} symmetry are out-of-plane oscillations that alternate similarly to B_{1g} and B_{2g} . Neither the basis for E_g nor the B_{1u} symmetry contains any dipole moment. Thus, bright out-of-plane plasmons of the quadramer have A_{2u} symmetry.

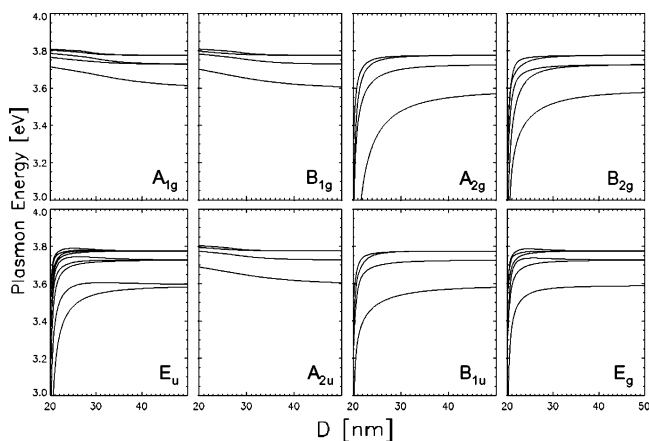


Figure 6. Plasmon energy vs characteristic separation for the nanosphere quadrumer described in Figure 4 up to $l = 3$ and classified by their dipolar symmetry. Plasmons corresponding to representations E_u can be excited by light polarized along the quadrumer plane and plasmons of A_{1u} symmetry can be excited by light polarized perpendicularly to the quadrumer plane.

Figure 6 shows the data from Figure 4a up to $l = 3$ classified by their dipolar symmetry. The plasmon modes of the quadrumer and trimer are qualitatively very similar. In each system, the in-plane bright modes have symmetries corresponding to two-dimensional representations that appear twice when the dipole representation is split into irreducible representations. Additionally, these modes red-shift greatly for close interparticle separations. The bright out-of-plane symmetries of each configuration correspond to modes that blue-shift slightly with decreasing nanoparticle separation. This situation is similar to the dimer, whose bright parallel modes red-shift greatly for closer separations but whose bright perpendicular modes blue-shift only slightly.^{18,19}

V. Discussion

In the following subsections we discuss some properties of the nanoparticle trimer and quadrumer relevant for experimental studies of these systems.

A. Optical Absorption. We have previously classified the dipolar plasmon modes as in-plane or out-of-plane excitations. The polarization of light used to excite bright out-of-plane modes is self-evident. However, the azimuthal dependence of the excitation of the bright in-plane plasmons has not been addressed. Our plasmon hybridization and FDTD investigations of the optical properties of the trimers and quadrumers reveal that the in-plane optical spectrum is independent of azimuthal polarization. Bright in-plane modes correspond to symmetries arising from the E' or E_u representations. Because these are two-dimensional representations, each plasmon mode has 2-fold degeneracy. Our studies show that the two physical excitations of a single energy form a planar basis that has the same dipole moment along either planar direction, and, thus, there is no azimuthal dependence on the excitation for an in-plane mode in the dipole limit.

This result can be proven rigorously for any system with such a degeneracy. We may use the trimer as an illustration. The E' states that are shown in Figure 2 correspond to two pairs that are each doubly degenerate in energy. The left pair has configurations that are lower energy, thus bonding, and the right pair has higher energy, antibonding configurations. The magnitude of the dipole moment is the same for all four modes, and each pair of degenerate energy states has dipole moments that are orthogonal to each other. We will denote the bonding

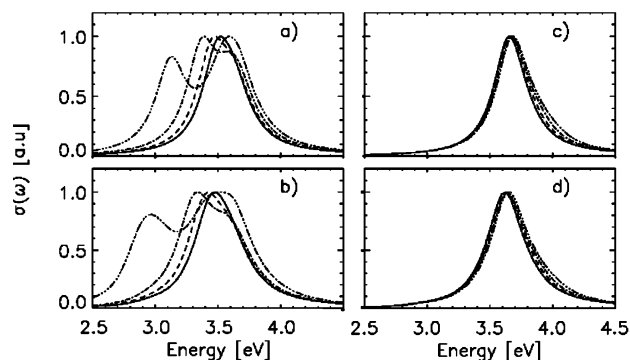


Figure 7. Optical absorption spectra of the $r = 10$ silver trimer for in-plane (a–b) and out-of-plane (c–d) excitations at four different separations. The separations are $D = 27$ (solid), $D = 25$ (dashed), $D = 23$ (dot–dashed), and $D = 21$ (triple dot–dashed). The top spectra are calculated using plasmon hybridization, and the bottom are calculated using FDTD. The FDTD calculations were made using a Drude dielectric function of silver with $\omega_B = 9.5$ eV, background polarization $\epsilon_\infty = 5$, and fwhm of 0.3 eV.

states as x_b and y_b where x and y refer to the direction of the dipole moment, and x_{ab} and y_{ab} will represent the antibonding states in a similar way. It is important to note that the proportion of a dipole component of a physical plasmon mode in relation to the higher order modes is the same between a state and its complement because the multipolar interactions between individual particle plasmons are symmetric, and the transformation to a symmetry-adapted basis does not mix multipolar orders. The dipole part of a physical plasmon mode is made of some linear combination of these four modes.

$$\Psi_{\text{dip}} = A(x_b \cos \alpha + y_b \sin \alpha) + B(x_{ab} \cos \beta + y_{ab} \sin \beta) \quad (7)$$

Here, α and β define the angles of the dipole moments from the bonding and antibonding components, respectively. The quantities A and B give the relative amount of bonding and antibonding states. A unique complementary state to the original dipole state may be constructed.

$$\Psi_{\text{dip}}^* = A^*(-x_b \sin \alpha + y_b \cos \alpha) + B^*(-x_{ab} \sin \beta + y_{ab} \cos \beta) \quad (8)$$

The energy of the dipole part depends of the ratio of the bonding and antibonding contributions, A/B or A^*/B^* . Because the complement of a physical plasmon is degenerate in energy and has the same magnitude of dipole components, however, the ratio must be the same for its complement, i.e., $A = A^*$ and $B = B^*$. Thus, both Ψ_{dip} and Ψ_{dip}^* have the same energy and dipole moments that span the plane with the same magnitude. Any degenerate energy made up of these states will have an azimuthally independent excitation. The quadrumer can clearly be combined into two pairs of states each with the same energy distinct from the other pair and the same dipole moment. The azimuthal independence of the in-plane plasmon modes can then be proven with the same argument.

Following the formalism developed in our previous dimer study¹⁹, the hybridization method can be used to calculate the optical absorption spectrum of both the trimer and the quadrumer. In Figures 7 and 8, we show a comparison between optical absorption spectra of the silver symmetric trimer and quadrumer, respectively, for different separations and calculated using the plasmon hybridization method and using FDTD simulations.^{26,27} The silver metal in FDTD is described by a Drude dielectric function with background dielectric of 5, broadening of 0.3 eV,

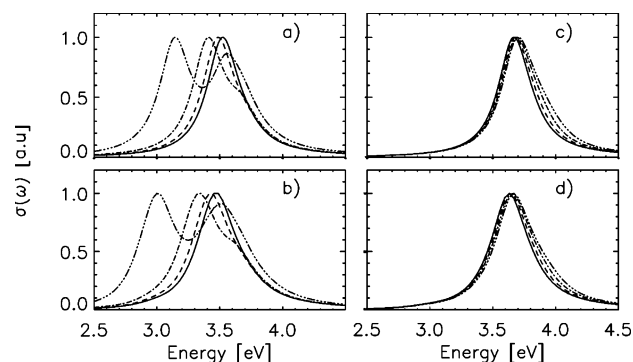


Figure 8. Optical absorption spectra of the $r = 10$ silver quadrumer for in-plane (a–b) and out-of-plane (c–d) excitations. The separations and method of calculation are the same as in Figure 7.

and $\omega_B = 9.5$ eV. We see a slight red-shift of the plasmon energies in FDTD when compared to plasmon hybridization. This is an effect of phase retardation and discrete errors introduced on the finite grid.^{26–28} Nevertheless, we see very good agreement between the two methods. The agreement of the in-plane spectra is better for the quadrumer system than the trimer because the geometry of a quadrumer is described better by the Cartesian grid utilized by the FDTD algorithm.

For in-plane excitations, light only couples to modes of E' (trimer) and E_u (quadrumer) symmetry. The higher l modes of this symmetry are dipole-active because of the hybridization with $l = 1$ plasmons. The situation is analogous to nanoparticle dimers where the admixture of dipolar nanoparticle plasmons make higher-order l dimer plasmons visible. For the trimer and quadrumer, the dipole active plasmon modes lie much closer in energy than for a dimer. A consequence of this is that a realistic plasmon broadening will prevent individual higher l plasmon modes from being resolved. A comparison of the spectra for $D = 21$ nm in Figures 7 and 8 with the spectra in Figures 1b and 4b reveals that the higher-energy peaks around 3.5 eV for in-plane excitations are built up by several smaller peaks corresponding to higher multipolar order trimer and quadrumer plasmon resonances.

It is interesting to compare the spectra for the trimer and quadrumer with the absorption spectrum from a dimer of the same interparticle separation $D = 21$ nm.¹⁹ For the dimer, the absorption spectrum reveals a strong feature at 3.08 eV whereas the lowest-energy visible resonances for the trimer and quadrumer lie around 3.12 and 3.14 eV, respectively. However, as shown in Figures 1a and 4a, the most strongly coupled plasmon mode is at 2.9 eV for the trimer, and 2.8 eV for the quadrumer. These correspond to A'_2 and A_{2g} modes, respectively. The red-shift of these nondipole-active modes compared to the dimer mode is due to the increased plasmonic couplings when more nanoparticles are present in the aggregate. Because these modes are made up of in-phase plasmon oscillations that are tangential to the center of the structure, they are dark. One can show that any symmetric ringlike combination of nanospheres should share this property. The lowest-energy mode of such a structure will have a symmetry with in-phase plasmon oscillations tangential to the center of the structure and no overall dipolar moment, and any bright modes will lie above this energy.

The reason the lowest-energy dipole-active quadrumer mode has higher energy than a similarly polarized dimer plasmon mode can be understood in very simple terms. The dipole active quadrumer mode corresponds approximately to two parallel bonding dipolar dimer plasmon modes. However, such a mode also has repulsively aligned (antibonding) dimer–dimer plasmon modes perpendicular to the excitation. A similar argument can

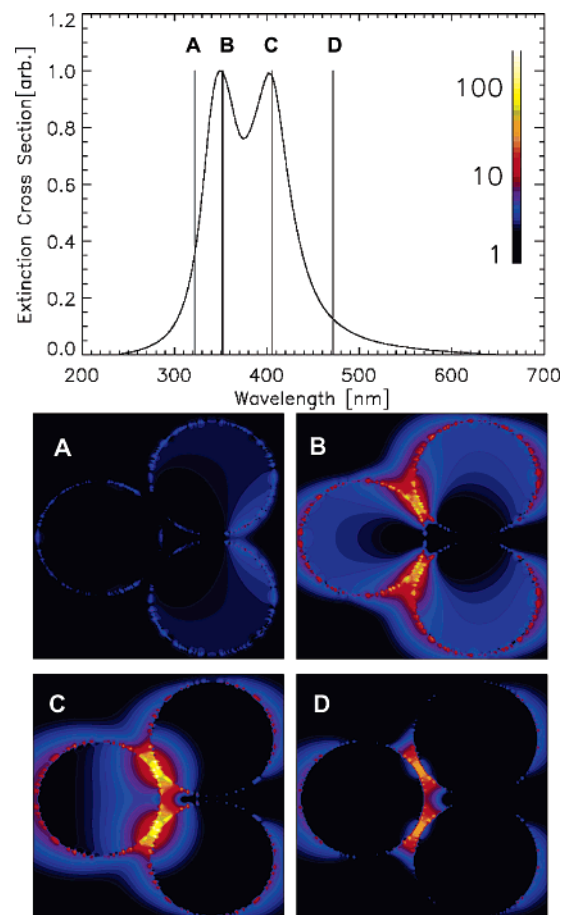


Figure 9. Electric field enhancements of a 10 nm silver trimer with a separation of 1 nm as calculated by FDTD. The top panel shows the extinction cross-section of this system, and the bottom four panels show the electric field enhancement for the wavelengths indicated by the legends in the top panel. The incoming light is polarized along the x -axis. The simulation uses a cell-size of 0.25 nm and the same parameters as Figure 7 for the silver metal.

be used to explain why the lowest-energy dipole-active trimer plasmon has larger energy than the lowest-energy dipole-active dimer mode.

In closing this subsection, we note that for a larger system, retardation effects can make the nondipole-active plasmon modes visible as was recently shown for a symmetric nanoshell dimer.²⁷

B. Electric Field Enhancements. In Figures 9 and 10, we show finite-difference time-domain calculations of the extinction spectra and local electric field enhancements at multiple wavelengths for a typical nanosphere trimer and nanosphere quadrumer. The dielectric function used to simulate the metal has the same broadening as in Figures 7 and 8. This value is approximately 1.5 times the experimentally observed broadening in the frequency range of interest. We chose this slightly larger broadening to eliminate the fine structure associated with excitation of the multitude of higher l dipole-active E modes that would be washed out by small nonsymmetric structural deformations of the trimer and quadrumer. However, this larger broadening also has the effect of lowering the maximum electromagnetic field enhancements. Therefore, the enhancements presented below should be taken as underestimations of the true enhancements of both systems.

The maximum electric field enhancement shown in each figure at the lowest energy peak (wavelength C) is approximately 120 for the trimer and 175 for the quadrumer. The

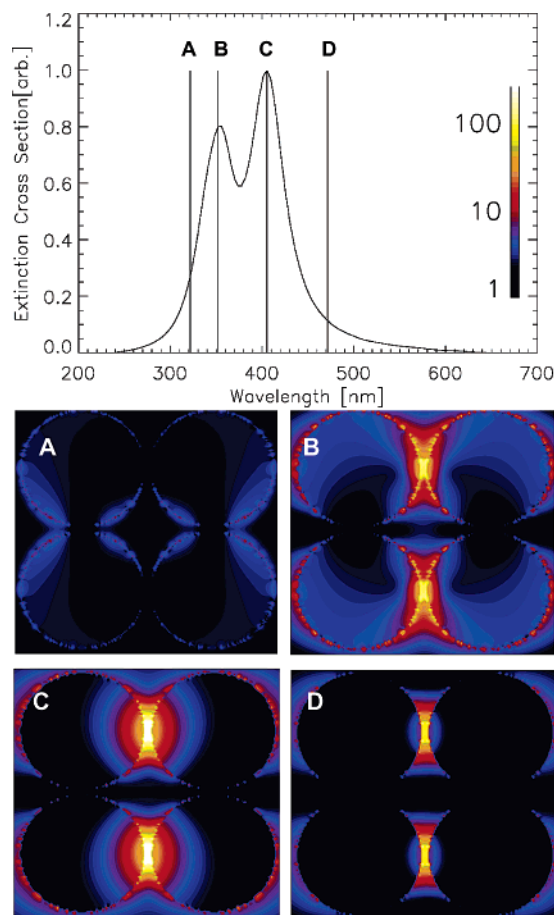


Figure 10. Electric field enhancements of a 10 nm silver quadramer with a separation of 1 nm as calculated by FDTD. (top) Extinction cross-section of this system and (bottom four) electric field enhancement for the wavelengths indicated by the legends in the top panel. The incoming light is polarized along the x -axis. The calculation parameters are the same as in Figure 9.

collective effects associated with the interactions of individual plasmons in different nanoparticles thus lead to very strong enhancements. The pattern of enhancement in Figure 9 bears a strong resemblance to the lower left dipole mode of the E' representation in Figure 2, whereas the enhancement pattern of the quadramer can be expressed as a linear combination of the E_u modes from Figure 5. The energy peak at wavelength C corresponds to the lowest energy $l = 1$ E' mode for the trimer and the lowest energy E_u mode for the quadramer, whereas the higher-energy peak contains several closely spaced $l = 2$ and higher order E resonances modes that become dipole-active due to plasmon hybridization. Finally, in both figures, the electromagnetic field enhancements are large at wavelength D, showing that significant enhancements also are induced for wavelengths extending far to the red of wavelength C.

C. Symmetry Breaking. Before ending this section, it is of interest to examine the role of symmetry breaking on the plasmon resonances. The plasmonic structure of the trimer and quadramer is not sensitive to small structural deformations that maintain the overall structure. Figure 11 shows how the optical absorption spectra of a trimer and a quadramer change when the structure of the respective system is significantly perturbed. All spectra are calculated using plasmon hybridization and correspond to an electric field excitation along the y -axis of the graph. The left panels show perturbations applied to a symmetric trimer at approximately 24.25 nm separation distance. The top panel corresponds to the unperturbed trimer, and the bottom

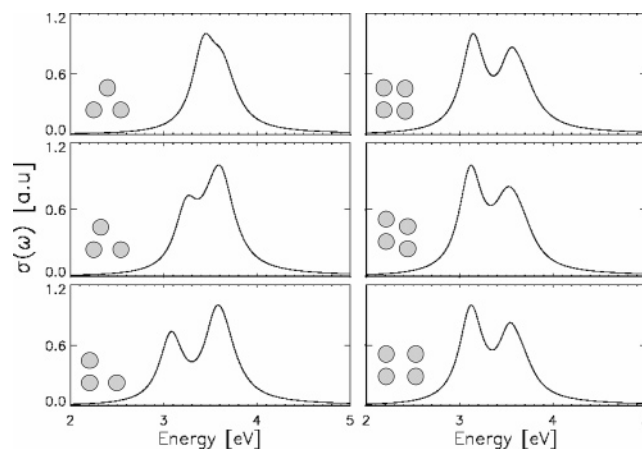


Figure 11. Plasmon hybridization calculations of the absorption spectra for a trimer and a quadramer with structural perturbations. The top panels correspond to the symmetric systems. The trimer is perturbed by moving the top sphere to be axially aligned with one of the other two spheres. The base symmetric trimer distance is chosen so that at maximum perturbation the gap distance between the closest two spheres is 1 nm. The quadramer is perturbed by moving the rightmost two spheres one radius down or one radius away from the center of the structure. The base symmetric quadramer distance is $D = 21$ nm. The incident light is polarized along the y -axis.

panel, the maximum perturbation, corresponds to an L-shaped structure. The middle panel corresponds to the trimer with the top sphere moved halfway between the symmetric trimer and the maximally perturbed system. The right panels show two different perturbations for a quadramer. The unperturbed system is shown in the top panel. The middle panel shows two adjacent spheres shifted parallel to their dimer axis by one radius, and the bottom shows them shifted perpendicularly and away from the center of the quadramer by one radius.

There is a large effect in the plasmonic structure of the trimer when the symmetry is broken in this manner. The symmetric linear combinations of the individual plasmon modes found earlier can no longer be used to describe the plasmons of the trimer. At maximum structural perturbation, the excitation, in effect, becomes a combination of modes from the dimer separated by 1 nm (approximately 3.08 eV) and an individual silver nanosphere (approximately 3.59 eV). The quadramer appears quite robust for the perturbations considered here as both peaks stay in the same approximate location and have similar relative heights. For the perturbation in the middle panel, plasmons between the two main bright modes become visible, leading to a slight broadening of the high-energy peak.

Finally, an experimentally relevant question involves the symmetry breaking introduced by the presence of a substrate. Unlike the free-standing clusters, trimers or quadrumers on a substrate correspond to C_{3v} and C_{4v} symmetries, respectively. Symmetry-adapted plasmons obtained from the D_{3h} and D_{4h} groups remain valid symmetry-adapted plasmons in these lower-symmetry subgroups. However, due to the absence of the horizontal mirror plane, the out-of-plane modes may fall into the same irreducible representations as in-plane ones. This means that the out-of-plane modes are no longer dipole forbidden and can become optically active. A similar effect has recently been discussed in the context of left-handed materials.²⁹

VI. Conclusion

The plasmon hybridization method has been extended to aggregates of nanoparticles of arbitrary symmetry. The plasmonic properties of the symmetric nanosphere trimer and

quadramer were calculated. We showed that, in analogy with molecular orbital theory, one can use group theory to understand the plasmon modes of each configuration as symmetry-specific linear combinations of plasmons from the individual particles. As the spheres move closer, there is a mixture of dipole plasmons with higher order modes of the same irreducible representation. This leads to higher energy plasmon modes being excitable by light at closer separations, but because the energies lie close to each other, broadening of the peaks will obscure some of these energies. With similar broadening, optical absorption spectra calculated by plasmon hybridization compare well with spectra obtained with FDTD.

Acknowledgment. We acknowledge valuable discussions with Drs. B. R. Johnson and N. J. Halas. This material is based upon work supported by, or in part by, the U. S. Army Research Laboratory and the U. S. Army Research Office under contract/grant number W911NF-04-1-0203, the Robert A. Welch Foundation under grants C-1222, and by the National Science Foundation under grants number EEC-0304097 and ECS-0421108.

References and Notes

- (1) Schatz, G. C.; Duynes, R. P. V. Electromagnetic mechanism of surface-enhanced spectroscopy. In *Handbook of Vibrational Spectroscopy*; Chalmers, J. M., Griffiths, P. R., Eds.; John Wiley: Chichester, 2002; pp 1–16.
- (2) Moskovits, M.; Tay, L.; Yang, J.; Haslett, T. *Topics Appl. Phys.* **2002**, 82, 215–226.
- (3) Kneipp, K.; Wang, Y.; Kneipp, H.; Perelman, L. T.; Itzkan, I.; Dasari, R. R.; Feld, M. S. *Phys. Rev. Lett.* **1997**, 78, 1667–1670.
- (4) Nie, S.; Emory, S. R. *Science* **1997**, 275, 1102–1106.
- (5) Michaels, A. M.; Nirmal, M.; Brus, L. E. *J. Am. Chem. Soc.* **1999**, 121, 9932–9939.
- (6) Wang, Z.; Pan, S.; Krauss, T. D.; Dui, H.; Rothberg, L. J. *Proc. Nat. Acad. Sci.* **2003**, 100, 8638–8643.
- (7) Jackson, J. B.; Halas, N. J. *Proc. Natl. Acad. Sci. U.S.A.* **2004**, 101, 17930–17935.
- (8) Xu, H.; Bjerneld, E. J.; Kall, M.; Borjesson, L. *Phys. Rev. Lett.* **1999**, 83, 4357–4360.
- (9) Moskovits, M.; Jeong, D. H. *Chem. Phys. Lett.* **2004**, 397, 91–95.
- (10) Talley, C. E.; Jackson, J. B.; Oubre, C.; Grady, N. K.; Hollars, C. W.; Lane, S. M.; Huser, T. R.; Nordlander, P.; Halas, N. J. *Nano Lett.* **2005**, 5, 1569–1574.
- (11) Kelly, K. L.; Coronado, E.; Zhao, L. L.; Schatz, G. C. *J. Phys. Chem. B* **2003**, 107, 668–677.
- (12) Li, K.; Stockman, M. I.; Bergman, D. J. *Phys. Rev. Lett.* **2003**, 91, 227402–1–4.
- (13) Schmeits, M.; Dambly, L. *Phys. Rev. B* **1991**, 44, 12706–12712.
- (14) Tamaru, H.; Kuwata, H.; Miyazaki, H. T.; Miyano, K. *Appl. Phys. Lett.* **2002**, 14, 348–3492.
- (15) Rechberger, W.; Hohenau, A.; Leitner, A.; Krenn, J. R.; Lamprecht, B.; Aussenegg, F. R. *Opt. Comm.* **2003**, 220, 137–144.
- (16) Su, K. H.; Wei, Q. H.; Zhang, X.; Mock, J. J.; Smith, D. R.; Schultz, S. *Nano Lett.* **2003**, 3, 1087–1090.
- (17) Futamata, M.; Maruyama, Y.; Ishikawa, M. *J. Phys. Chem. B* **2003**, 107, 7607–7617.
- (18) Nordlander, P.; Oubre, C.; Prodan, E.; Li, K.; Stockman, M. I. *Nano Lett.* **2004**, 4, 899–903.
- (19) Brandl, D. W.; Oubre, C.; Nordlander, P. *J. Chem. Phys.* **2005**, 123, 024701.
- (20) Prodan, E.; Radloff, C.; Halas, N. J.; Nordlander, P. *Science* **2003**, 302, 419–422.
- (21) Prodan, E.; Nordlander, P. *J. Chem. Phys.* **2004**, 120, 5444–5454.
- (22) Nordlander, P.; Prodan, E. *Nano Lett.* **2004**, 4, 2209–2213.
- (23) Le, F.; Lwin, N. Z.; Steele, J. M.; Kall, M.; Halas, N. J.; Nordlander, P. *Nano Lett.* **2005**, 5, 2009–2013.
- (24) Cotton, F. A. *Chemical Applications of Group Theory*, 3rd ed.; Wiley-Interscience: United States, 1990.
- (25) Tinkham, M. *Group Theory and Quantum Mechanics*; Dover Publications: United States, 2003.
- (26) Oubre, C.; Nordlander, P. *J. Phys. Chem. B* **2004**, 108, 17740–17747.
- (27) Oubre, C.; Nordlander, P. *J. Phys. Chem. B* **2005**, 109, 10042–10051.
- (28) Ditkowski, A.; Dridi, K.; Hesthaven, J. S. *J. Comput. Phys.* **2000**, 170, 39–80.
- (29) Grigorenko, A. N.; Geim, A. K.; Giessen, H. F.; Zhang, Y.; Firsov, A. A.; Khrushchev, I. Y.; Petrovic, J. *Nature* **2005**, 438, 335–338.